Communications in Physics, Vol. 28, No. 1 (2018), pp. 1-19
DOI:10.15625/0868-3166/28/1/11722

Invited Paper

COPING WITH NOISE IN JOINT REMOTE PREPARATION OF A GENERAL TWO-QUBIT STATE BY USING NONMAXIMALLY ENTANGLED QUANTUM CHANNEL

LE THANH DAT[1], NGUYEN VAN HOP[2] AND NGUYEN BA AN[1,3,†]

[1]*Thang Long Institute of Mathematics and Applied Sciences, Thang Long University, Nghiem Xuan Yem, Hoang Mai, Hanoi, Vietnam*

[2]*Department of Physics, Hanoi National University of Education, 136 Xuan Thuy, Cau Giay, Hanoi, Vietnam*

[3]*Institute of Physics, Vietnam Academy of Science and Technology, 18 Hoang Quoc Viet, Cau Giay, Hanoi, Vietnam*

[†]*E-mail:* nban@iop.vast.ac.vn

Received 17 February 2018
Accepted for publication 17 March 2018
Published 26 March 2018

Abstract. *Noise is unavoidable in practice and its presence makes quantum protocols imperfect. In this paper we consider a way to cope with typical types of noise in joint remote preparation of an arbitrary 2-qubit state. The idea is to use nonmaximally (instead of maximally) entangled states as the initial quantum channel. Because noise changes the initial quantum channel we can beforehand tailor it to be nonmaximally entangled by introducing free parameters which, depending on given types of noise, can be controlled so that due to the affect of noise the initial quantum channel becomes closest to the maximally entangled one, thus optimizing the performance of the joint remote state preparation protocol. The dependence of the optimal averaged fidelities on the strength of various types of noise is represented by phase diagrams that clearly separate the quantum domain from the classical one.*

Keywords: joint remote state preparation, two-qubit state, noise.

Classification numbers: 03.65.Ud.

I. INTRODUCTION

Multiparty remote state preparation [1] or joint remote state preparation (JRSP) [2] or collective remote state preparation [3] are three formally different names of the same quantum protocol which we call JRSP in this paper. JRSP's primary aim is to prepare by means of local operation and classical communication (LOCC) a quantum state at a distant location by a group of people (called preparers) who are spatially separated. The salient distinction between JRSP and remote state preparation (RSP) (see, e.g. [4]) is that in RSP there is only one preparer who knows the full classical information of the state to be prepared, while in JRSP there are more than one preparer and each of them just holds a partial classical information of the to-be-prepared state so none of them can learn the full secrecy encoded in the quantum state, thus ensuring the desired security of the state preparation process. JRSP has been received much attention with regards to different types of quantum states and nonlocal quantum channels [5–23]. The key strategy in JRSP to achieve perfection (i.e., with both its success probability and fidelity equal to 1) is to suitably split information of the input state and employ adequate measurement procedures in which the measurements are done sequentially in an adaptive manner: outcome of a previous measurement decides the basis of a next one [10,16,19,20]. The experimental perspective of JRSP has also been addressed as well [24,25]. However, JRSP protocols in particular or quantum protocols in general are perfect only in ideal conditions. In practice there are many obstacles that prevent quantum protocols from being perfect. One of such obstacles is noises originated from surrounding environment with which quantum states of interest interact. The commonly recognized consequence of noise is degradation of entanglement degree of the quantum channel and therefore reduces the quality of the protocol. Depending on type and strength of noises the initially intended entanglement may vanish suddenly or asymptotically [26,27] as time/distance grows. An efficient method to cope with noises is entanglement distillation that transforms a large number of previously shared less entangled states into a smaller number of maximally entangled ones using only LOCC [28] - [30]. Another method to protect entanglement is based on weak measurements [31, 32]. The drawback of both techniques is that the success probability is less than 1. Several studies related to improving quantum teleportation protocol under the effect of noise have exploited quantum distillation [28, 33] and weak measurements [34, 35]. However, when there is only one copy of the entangled state the above methods do not apply. In this situation one may intentionally distribute nonmaximally (instead of maximally) entangled states characterized by some parameters which can be controlled so that the protocol performance is optimal under certain types of noise. Such an approach to cope with noises in quantum teleportation has recently been developed [36–41].

JRSP in noisy scenarios has also been investigated through solving Lindblad master equations [42, 43] or using Kraus operators [44–46]. Recently, JRSP of an arbitrary 1-qubit state in the presence of noises has been studied [47] in which the initial quantum channel and the steps of performance are suitably designed to optimize the fidelity. Our aim in this paper is to optimize noisy JRSP of an arbitrary 2-qubit state. The types of noise to be dealt with are those caused by the bit-flip, phase-flip, depolarizing and amplitude-damping mechanisms [48, 49]. By means of adjustment in the standard JRSP protocol, the averaged fidelities are optimized and then analyzed through their phase diagrams. The results show that the protocol with amplitude-damping or phase-flip noise is more robust than with the other noises. In case of bit-flip noise the second preparer, who produces the quantum channel, can apply the Pauli operator σ_x to obtain the desired

fidelity at a large value of noise strength. Some specific scenarios, in addition, show that lesser initial quantum entanglement or greater noise strength can boost the quality of JRSP. From these results, we categorize more precisely two ways for the optimization according to their features. In Sec. **II**, we briefly describe JRSP of an arbitrary 2-qubit state in density operator representation. We then optimize the values of the averaged fidelities obtained in various scenarios of noises and analyze their phase diagrams in Sec. **III**. Finally, Sec. **IV** is devoted to the conclusions.

II. DENSITY OPERATOR REPRESENTATION

Let Alice, Bob and Charlie be 3 remote parties. Alice and Bob are assigned a task of jointly preparing for Charlie a 2-qubit state of the most general form

$$|\psi\rangle = \lambda_0 |00\rangle + \lambda_1 e^{i\varphi_1} |01\rangle + \lambda_2 e^{i\varphi_2} |10\rangle + \lambda_3 e^{i\varphi_3} |11\rangle , \tag{1}$$

where $\varphi_j \in [0, 2\pi]$ and λ_j are real numbers satisfying the condition $\sum_{i=0}^{3} \lambda_i^2 = 1$. The full classical information characterizing state $|\psi\rangle$ (i.e., the phases φ_j and the amplitudes λ_j) is divided between Alice and Bob in such a way that Alice holds the values of $\{\lambda_0, \lambda_1, \lambda_2, \lambda_3\}$ while Bob those of $\{\varphi_1, \varphi_2, \varphi_3\}$. Since the 3 parties are working in 3 spatially separated labs and allowed to do only LOCC, to fulfill the task they must priorly share a quantum channel described by a density matrix ρ_{123456} which is made up at least of six qubits. Let us label $1,2$ ($3,4$ and $5,6$) the qubits belonging to Alice (Bob and Charlie). The general procedure to perform JRSP goes as follows.

First, Alice measures qubits 1 and 2 in the basis $\{|\omega_{kl}\rangle_{12}; k,l \in \{0,1\}\}$,

$$|\omega_{kl}\rangle_{12} = \sum_{m,n=0}^{1} U_{kl,mn} |mn\rangle_{12} , \tag{2}$$

where $U_{kl,mn}$ are matrix elements of U, a 4×4 unitary matrix, which is determined by the amplitudes $\{\lambda_j\}$. After obtaining an outcome kl (i.e., finding a state $|\omega_{kl}\rangle_{12}$), Alice announces the values of k and l. As an immediate consequence of this, the state of ρ_{123456} reduces to an entangled state now connecting only Bob and Charlie

$$\rho_{123456} \to \rho_{3456}^{(kl)} = \frac{{}_{12}\langle\omega_{kl}|\rho_{123456}|\omega_{kl}\rangle_{12}}{P^{(kl)}} \tag{3}$$

with $P^{(kl)} = Tr({}_{12}\langle\omega_{kl}|\rho_{123456}|\omega_{kl}\rangle_{12})$ the probability that Alice obtains the outcome kl.

Next, based on the announced values of k and l, Bob applies on qubits 3 and 4 a unitary operator $T_{34}^{(kl)}$ to transform $\rho_{3456}^{(kl)}$ into an appropriate form and then measures qubits 3 and 4 in the basis $\{|\sigma_{mn}\rangle_{34}; m,n \in \{0,1\}\}$,

$$|\sigma_{mn}\rangle_{34} = \sum_{p,q=0}^{1} V_{mn,pq} |pq\rangle_{34} , \tag{4}$$

where $V_{mn,pq}$ are matrix elements of V, a 4×4 unitary matrix, which depends on the phase information $\{\varphi_j\}$. If Bob's result is mn (i.e., he finds a state $|\sigma_{mn}\rangle_{34}$), he publicly broadcasts the values of m and n. The state $\rho_{3456}^{(kl)}$ is further collapsed into

$$\rho_{3456}^{(kl)} \to \rho_{56}^{(klmn)} = \frac{{}_{34}\left\langle\sigma_{mn}\right|T_{34}^{(kl)}\rho_{3456}^{(kl)}T_{34}^{(kl)\dagger}\left|\sigma_{mn}\right\rangle_{34}}{P^{(klmn)}} \tag{5}$$

with $P^{(klmn)} = Tr\left({}_{34}\left\langle \sigma_{mn}\right| T_{34}^{(kl)} \rho_{3456}^{(kl)} T_{34}^{(kl)\dagger} \left|\sigma_{mn}\right\rangle_{34}\right)$ the probability that Bob obtains the outcome mn.

Finally, according to the values of kl and mn announced by Alice and Bob, Charlie applies on $\rho_{56}^{(klmn)}$ an appropriate unitary operator $R_{56}^{(klmn)}$ to obtain the state

$$\widetilde{\rho}_{56}^{(klmn)} = R_{56}^{(klmn)} \rho_{56}^{(klmn)} R_{56}^{(klmn)\dagger}. \tag{6}$$

For a given state $|\psi\rangle$ the quality of the JRSP described above is determined by the fidelity

$$F = \sum_{k,l,m,n=0}^{1} P^{(kl)} P^{(klmn)} \langle\psi| \widetilde{\rho}^{(klmn)} |\psi\rangle . \tag{7}$$

Since F is a function of amplitude and phase information of the state to be prepared, it is relevant to average F over all the input information, yielding the so-called averaged fidelity $\overline{F}$ which is state-independent. To calculate $\overline{F}$ we set

$$\left.\begin{array}{ll} \lambda_0 = \cos\eta_3, & \lambda_1 = \sin\eta_3 \cos\eta_2, \\ \lambda_2 = \sin\eta_3 \sin\eta_2 \cos\eta_1, & \lambda_3 = \sin\eta_3 \sin\eta_2 \sin\eta_1 \end{array}\right\} \tag{8}$$

with $\eta_i \in [0, \pi/2]$ and have [50]

$$\overline{F} = \frac{3!}{\pi^3} \int_0^{\frac{\pi}{2}} d\eta_1 \int_0^{\frac{\pi}{2}} d\eta_2 \int_0^{\frac{\pi}{2}} d\eta_3 \int_0^{2\pi} d\varphi_1 \int_0^{2\pi} d\varphi_2 \int_0^{2\pi} d\varphi_3 \prod_{j=1}^{3} F \cos\eta_j . (\sin\eta_j)^{2j-1}. \tag{9}$$

III. EFFECT OF NOISES

Let us first consider the ideal scenario when the quantum channel is noiseless. The channel we consider consists of 2 maximally entangled Greenberger-Horne-Zeilinger (GHZ) states

$$|Q\rangle_{135246} = |GHZ_+\rangle_{135} \otimes |GHZ_+\rangle_{246}, \tag{10}$$

where

$$|GHZ_\pm\rangle_{abc} = \frac{1}{\sqrt{2}} \left(|000\rangle \pm |111\rangle\right)_{abc}. \tag{11}$$

The unitary matrix U in Eq. (2) that is relevant to Alice's measurement basis can be explicitly chosen in the form

$$U = \begin{pmatrix} \lambda_0 & \lambda_1 & \lambda_2 & \lambda_3 \\ -\lambda_1 & \lambda_0 & -\lambda_3 & \lambda_2 \\ -\lambda_2 & \lambda_3 & \lambda_0 & -\lambda_1 \\ -\lambda_3 & -\lambda_2 & \lambda_1 & \lambda_0 \end{pmatrix}. \tag{12}$$

The operator $T_{34}^{(kl)}$ mentioned in the second step of Bob's operation after hearing Alice's announcement is

$$T_{34}^{(kl)} = Z_3^k X_3^k \otimes Z_4^{k\oplus l} X_4^l \tag{13}$$

with X_j (Z_j) the standard 2×2 Pauli matrix σ_x (σ_z) acting on qubit j and $\oplus$ the addition mod 2. As for the unitary matrix V in Eq. (4) that generates Bob's measurement basis, it is now

unambiguously designed as

$$V=\frac{1}{2}\begin{pmatrix} 1 & e^{-i\varphi_1} & e^{-i\varphi_2} & e^{-i\varphi_3} \\ 1 & -e^{-i\varphi_1} & e^{-i\varphi_2} & -e^{-i\varphi_3} \\ 1 & e^{-i\varphi_1} & -e^{-i\varphi_2} & -e^{-i\varphi_3} \\ 1 & -e^{-i\varphi_1} & -e^{-i\varphi_2} & e^{-i\varphi_3} \end{pmatrix}. \tag{14}$$

Then the operators $R_{56}^{(klmn)}$ mentioned above for Charlie's operation can be constructed as

$$R_{56}^{(klmn)}=Z_5^m X_5^k \otimes Z_6^n X_6^l. \tag{15}$$

It is easy to verify that $P^{(kl)}=P^{(klmn)}=1/4$ and $F^{(klmn)}=1$ for any k,l,m,n depending neither on $\{\lambda_i\}$ nor on $\{\varphi_j\}$. That implies perfect JRSP which has both the success probability and the fidelity equal to 1.

Now consider practical scenarios when the quantum channel is noisy. Since noisy environment has tendency to make a maximal entanglement nonmaximal, to cope with such disentanglement process one might start with a nonmaximally entangled channel characterized by some free parameters which, depending on the type of noise, can be tailored so that after surviving the action of noise the initial nonmaximally entangled channel becomes more entangled or even near-maximally entangled, resulting in a better quality compared with starting with maximally entangled channel. Here, instead of (10), we start with the quantum channel of the form

$$|Q(\theta)\rangle_{135246}=|GHZ_+\rangle_{135}\otimes|GHZ_+(\theta)\rangle_{246}, \tag{16}$$

where

$$|GHZ_\pm(\theta)\rangle_{abc}=(\cos\theta\,|000\rangle\pm\sin\theta\,|111\rangle)_{abc}. \tag{17}$$

The angle θ is introduced in Eq. (16) as a parameter whose value can be chosen to optimize the JRSP depending on the noise type. The matrix U is kept unchanged as in Eq. (12), but the matrix V differs from that in Eq. (14), namely,

$$V\to\widetilde{V}=\frac{1}{\sqrt{2}}\begin{pmatrix} \cos\xi & e^{-i\varphi_1}\cos\xi & e^{-i\varphi_2}\sin\xi & e^{-i\varphi_3}\sin\xi \\ \cos\xi & -e^{-i\varphi_1}\cos\xi & e^{-i\varphi_2}\sin\xi & -e^{-i\varphi_3}\sin\xi \\ \sin\xi & e^{-i\varphi_1}\sin\xi & -e^{-i\varphi_2}\cos\xi & -e^{-i\varphi_3}\cos\xi \\ \sin\xi & -e^{-i\varphi_1}\sin\xi & -e^{-i\varphi_2}\cos\xi & e^{-i\varphi_3}\cos\xi \end{pmatrix}, \tag{18}$$

where we again introduce another parameter ξ for the purpose of optimizing the JRSP (see later).

Noise may arise by various mechanisms. Here, we study 4 typical mechanisms which are commonly referred to as bit-flip noise (B), phase-flip noise (P), amplitude-damping noise (A) and depolarizing noise (D). Effect of these noises can be described in terms of Kraus operators [48]. For the 3 first types of above-mentioned noise mechanisms there are 2 Kraus operators:

$$K_1^{(B)}(p_B) = \sqrt{1-p_B}I, K_2^{(B)}(p_B)=\sqrt{p_B}X, \tag{19}$$

$$K_1^{(P)}(p_P) = \sqrt{1-p_P}I, K_2^{(P)}(p_P)=\sqrt{p_P}Z, \tag{20}$$

$$K_1^{(A)}(p_A) = \begin{pmatrix} 1 & 0 \\ 0 & \sqrt{1-p_A} \end{pmatrix}, K_2^{(A)}(p_A)=\begin{pmatrix} 0 & \sqrt{p_A} \\ 0 & 0 \end{pmatrix}, \tag{21}$$

while for the last noise type the number of Kraus operators is 4 :

$$\begin{aligned} K_1^{(D)}(p_D) &= \sqrt{1-\frac{3}{4}p_D}I, K_2^{(D)}(p_D) = \sqrt{\frac{1}{4}p_D}X, \\ K_3^{(D)}(p_D) &= \sqrt{\frac{1}{4}p_D}Y, K_4^{(D)}(p_D) = \sqrt{\frac{1}{4}p_D}Z, \end{aligned} \tag{22}$$

where Y is the standard Pauli matrix σ_y. In Eqs. (19) - (22) p_J measures strength of the J-type noise. Suppose that each of the 6 qubits $1,2,3,4,5$ and 6 of the initial quantum channel (16) independently suffers a type of noise, then the overall influence of noises is modeled by virtue of a superoperator that takes the state of the initial quantum channel $\rho_{135246}^{(0)}(\theta) = \rho_{135}^{(0)} \otimes \rho_{246}^{(0)}(\theta)$, with $\rho_{135}^{(0)} = |GHZ_+\rangle_{135}\langle GHZ_+|$ and $\rho_{246}^{(0)}(\theta) = |GHZ_+(\theta)\rangle_{246}\langle GHZ_+(\theta)|$, into a decohered state

$$\rho_{135246}^{(\alpha\gamma\epsilon\beta\delta\zeta)}(\theta) = \rho_{135}^{(\alpha\gamma\epsilon)} \otimes \rho_{246}^{(\beta\delta\zeta)}(\theta), \tag{23}$$

$$\begin{aligned} \rho_{135}^{(\alpha\gamma\epsilon)} &= \sum_{i=1}^{N_\alpha}\sum_{k=1}^{N_\gamma}\sum_{m=1}^{N_\epsilon} K_i^{(\alpha)}(p_{1\alpha}) \otimes K_k^{(\gamma)}(p_{3\gamma}) \otimes K_m^{(\epsilon)}(p_{5\epsilon}) \\ &\quad .\rho_{135}^{(0)}. \left[K_i^{(\alpha)}(p_{1\alpha}) \otimes K_k^{(\gamma)}(p_{3\gamma}) \otimes K_m^{(\epsilon)}(p_{5\epsilon})\right]^\dagger, \end{aligned} \tag{24}$$

$$\begin{aligned} \rho_{246}^{(\beta\delta\zeta)}(\theta) &= \sum_{j=1}^{N_\beta}\sum_{\ell=1}^{N_\delta}\sum_{n=1}^{N_\zeta} K_j^{(\beta)}(p_{2\beta}) \otimes K_\ell^{(\delta)}(p_{4\delta}) \otimes K_n^{(\zeta)}(p_{6\zeta}) \\ &\quad .\rho_{246}^{(0)}(\theta). \left[K_j^{(\beta)}(p_{2\beta}) \otimes K_\ell^{(\delta)}(p_{4\delta}) \otimes K_n^{(\zeta)}(p_{6\zeta})\right]^\dagger. \end{aligned} \tag{25}$$

In Eqs. (24) and (25) $K_j^{(\alpha)}(p_{1\alpha})$ and $p_{1\alpha}\,(0 \le p_{1\alpha} \le 1)$ are the j^{th} Kraus operator and the noise strength of the α-type noise, $\alpha \in \{B,P,A,D\}$, that affects qubit 1 and N_α is the number of the α-type noise Kraus operators. Similar notations hold for $K_j^{(\beta)}(p_{2\beta})$, $K_k^{(\gamma)}(p_{3\gamma})$, $K_\ell^{(\delta)}(p_{4\delta})$, $K_m^{(\epsilon)}(p_{5\epsilon})$, $K_n^{(\zeta)}(p_{6\zeta})$, $p_{2\beta}$, $p_{3\gamma}$, $p_{4\delta}$, $p_{5\epsilon}$, $p_{6\zeta}$ and $N_\beta, N_\gamma, N_\delta, N_\epsilon, N_\zeta$. The noisy scenario of our interest is as follows. Let Bob be the one who produces the quantum channel (16) at his site. Afterwards, he sends qubits 1 and 2 through an α-type noisy channel to Alice and qubits 5 and 6 through a γ-type noisy channel to Charlie, while keeping qubits 3 and 4 with himself. For simplicity, we assume $p_{1\alpha} = p_{2\alpha} = \mu_\alpha$ and $p_{5\gamma} = p_{6\gamma} = \nu_\gamma$ so $\rho_{135246}^{(\alpha\gamma\epsilon\beta\delta\zeta)}(\theta)$ simplifies to

$$\begin{aligned} \rho_{135246}^{(\alpha\gamma)}(\theta) &= \sum_{i=1}^{N_\alpha}\sum_{k=1}^{N_\gamma} K_i^{(\alpha)}(\mu_\alpha) \otimes I \otimes K_k^{(\gamma)}(\nu_\gamma).\rho_{135}^{(0)}. \left[K_i^{(\alpha)}(\mu_\alpha) \otimes I \otimes K_k^{(\gamma)}(\nu_\gamma)\right]^\dagger \\ &\quad \otimes \sum_{j=1}^{N_\alpha}\sum_{\ell=1}^{N_\gamma} K_j^{(\alpha)}(\mu_\alpha) \otimes I \otimes K_\ell^{(\gamma)}(\nu_\gamma).\rho_{246}^{(0)}(\theta). \left[K_j^{(\alpha)}(\mu_\alpha) \otimes I \otimes K_\ell^{(\gamma)}(\nu_\gamma)\right]^\dagger. \end{aligned} \tag{26}$$

First, consider the situation when $\alpha = B$ and $\gamma \in \{B,P,A,D\}$. Following the procedure outlined in the previous section we have calculated various averaged fidelities $\overline{F}_{B\gamma}$ which have the

explicit expressions as

$$\begin{aligned}
\overline{F}_{BB} &= \frac{2}{5}+\frac{1}{5}\left[\mu_B\left(2\nu_B-1\right)-\nu_B\right]\left[\mu_B\left(2\nu_B-1\right)-\nu_B+2\right] \\
&\quad +\frac{1}{80}\left[(\pi^2-16)\mu_B+16\right]\left(\nu_B-1\right)^2\left(\sin 2\xi+\sin 2\theta\right) \\
&\quad +\frac{1}{40}\left[8-(16-\pi^2)(\mu_B-\mu_B^2)\right]\left(\nu_B-1\right)^2\sin 2\xi\sin 2\theta, \qquad (27) \\
\overline{F}_{BP} &= \frac{2}{5}+\frac{1}{5}\left(\mu_B-2\right)\mu_B+\frac{1}{80}\left[(\pi^2-16)\mu_B+16\right]\left(1-2\nu_P\right)\left(\sin 2\xi+\sin 2\theta\right) \\
&\quad +\frac{1}{40}\left[8-(16-\pi^2)(\mu_B-\mu_B^2)\right]\left(2\nu_P-1\right)^2\sin 2\xi\sin 2\theta, \qquad (28) \\
\overline{F}_{BA} &= \frac{2}{5}+\frac{1}{20}\left[2\mu_B\left(\nu_A-1\right)-\nu_A\right]\left[2\mu_B\left(\nu_A-1\right)-\nu_A+4\right] \\
&\quad +\frac{1}{20}(1-2\mu_B)\nu_A\left[2\mu_B\left(\nu_A-1\right)-\nu_A+2\right]\cos 2\theta \\
&\quad +\frac{1}{160}\left[(\pi^2-16)\mu_B+16\right]\sqrt{1-\nu_A}(2-\nu_A)\left(\sin 2\xi+\sin 2\theta\right) \\
&\quad +\frac{1}{160}\left[(\pi^2-16)\mu_B+16\right]\sqrt{1-\nu_A}\nu_A\sin 2\xi\cos 2\theta \\
&\quad +\frac{1}{40}\left[8-(16-\pi^2)(\mu_B-\mu_B^2)\right]\left(1-\nu_A\right)\sin 2\xi\sin 2\theta, \qquad (29) \\
\overline{F}_{BD} &= \frac{2}{5}+\frac{1}{20}\left[2\mu_B\left(\nu_D-1\right)-\nu_D\right]\left[2\mu_B\left(\nu_D-1\right)-\nu_D+4\right] \\
&\quad +\frac{1}{160}\left[(\pi^2-16)\mu_B+16\right]\left(\nu_D-2\right)\left(\nu_D-1\right)\left(\sin 2\xi+\sin 2\theta\right) \\
&\quad +\frac{1}{40}\left[8-(16-\pi^2)(\mu_B-\mu_B^2)\right]\left(1-\nu_D\right)^2\sin 2\xi\sin 2\theta. \qquad (30)
\end{aligned}$$

As usually encountered, the fidelity depends on the noise type and decreases with increasing noise strength. However, as will be seen shortly, by using partially entangled quantum channel (16) and the modified matrix (18) we could somehow cope with the decoherence effect. This is thanks to the fact that, conditioned on given noise type and strength, one can choose the values of θ and ξ so that the averaged fidelity is optimal.

From Eqs. (27) and (30), the coefficients of both $(\sin 2\xi+\sin 2\theta)$ and $\sin 2\xi\sin 2\theta$ are always positive so the optimal values of θ and ξ that maximize $\overline{F}_{BB}$ and $\overline{F}_{BD}$ are

$$\theta_{opt}^{(BB)}=\xi_{opt}^{(BB)}=\theta_{opt}^{(BD)}=\xi_{opt}^{(BD)}=\frac{\pi}{4}. \qquad (31)$$

As for $\overline{F}_{BP}$ in Eq. (28), the coefficient of $\sin 2\xi\sin 2\theta$ is always positive, but the sign of the coefficient of $(\sin 2\xi+\sin 2\theta)$ changes at $\nu_P=1/2$. Thus, the optimal value of $\overline{F}_{BP}$ is achieved when

$$\theta_{opt}^{(BP)}=\xi_{opt}^{(BP)}=\begin{cases}\pi/4 & \text{for } \nu_P<1/2, \\ -\pi/4 & \text{for } \nu_P>1/2.\end{cases} \qquad (32)$$

The remaining case of $\overline{F}_{BA}$ in Eq. (29) is much more complicated. Although it is easy to find out that $\xi_{opt}^{(BA)} = \pi/4$, the value of $\theta_{opt}^{(BA)}$ must be determined from the conditions $\partial\overline{F}_{BA}/\partial\,\theta|_{\theta=\theta_{opt}^{(BA)}} = 0$ and $\partial^2\overline{F}_{BA}/\partial^2\theta|_{\theta=\theta_{opt}^{(BA)}} < 0$, which yield

$$\theta_{opt}^{(BA)} = \frac{1}{2}\arctan\frac{4\left[8-(16-\pi^2)\left(\mu_B-\mu_B^2\right)\right](1-\nu_A)+\left[16-(16-\pi^2)\mu_B\right]\sqrt{1-\nu_A}\,(2-\nu_A)}{\left[(\pi^2-16)\mu_B+16\right]\sqrt{1-\nu_A}\nu_A+8\,(1-2\mu_B)\,\nu_A\left[2-\nu_A-2\mu_B\,(1-\nu_A)\right]} \tag{33}$$

with $\sin 2\theta_{opt}^{(BA)} > 0$ and $\cos 2\theta_{opt}^{(BA)} > 0$ for μ_B, ν_A satisfying the inequality

$$\left[(\pi^2-16)\mu_B+16\right]\sqrt{1-\nu_A}\nu_A+8\,(1-2\mu_B)\,\nu_A\left[2-\nu_A-2\mu_B\,(1-\nu_A)\right] > 0 \tag{34}$$

or $\sin 2\theta_{opt}^{(BA)} > 0$ and $\cos 2\theta_{opt}^{(BA)} < 0$ for μ_B, ν_A satisfying the inequality

$$\left[(\pi^2-16)\mu_B+16\right]\sqrt{1-\nu_A}\nu_A+8\,(1-2\mu_B)\,\nu_A\left[2-\nu_A-2\mu_B\,(1-\nu_A)\right] < 0. \tag{35}$$

With such values of $\theta_{opt}^{(B\gamma)}$ and $\xi_{opt}^{(B\gamma)}$ the optimal averaged fidelities $\overline{F}_{B\gamma,opt}$ become

$$\begin{aligned}
\overline{F}_{BB,opt} &= \frac{2}{5}+\frac{1}{40}\Big\{2\mu_B\,(\nu_B-1)\left[(\pi^2-32)\nu_B-\pi^2+24\right]+8(4\nu_B^2-8\nu_B+3)\\
&\quad+\mu_B^2\left[(48-\pi^2)\nu_B^2-2(32-\pi^2)\nu_B+24-\pi^2\right]\Big\}, \qquad (36)\\
\overline{F}_{BP,opt} &= \frac{2}{5}+\frac{1}{40}\Big\{8\mu_B\,(\mu_B-2)+\left[(\pi^2-16)\mu_B+16\right]|1-2\nu_P|\\
&\quad+\left[8-(\pi^2-16)\left(\mu_B^2-\mu_B\right)\right](1-2\nu_P)^2\Big\}, \qquad (37)\\
\overline{F}_{BD,opt} &= \frac{2}{5}+\frac{1}{80}\Big\{48+12\nu_D\,(3\nu_D-8)-2(\pi^2-24)\mu_B^2\,(\nu_D-1)^2\\
&\quad+\mu_B\,(\nu_D-1)\left[(3\pi^2-64)\nu_D-4\pi^2+96\right]\Big\}, \qquad (38)\\
\overline{F}_{BA,opt} &= \frac{2}{5}+\frac{1}{160}\Big\{\left[(16-\pi^2)\mu_B-16\right]\sqrt{1-\nu_A}\,(\nu_A-2)\\
&\quad+8\left[2\mu_B(\nu_A-1)-\nu_A\right]\left[2\mu_B\,(\nu_A-1)-\nu_A+4\right]\Big\}\\
&\quad+\frac{1}{160}\Bigg\{\Big\{4\left[8-(16-\pi^2)(\mu_B-\mu_B^2)\right](1-\nu_A)\\
&\quad+\left[16-(16-\pi^2)\mu_B\right]\sqrt{1-\nu_A}(2-\nu_A)\Big\}^2\\
&\quad+\Big\{8(1-2\mu_B)\nu_A\left[2\mu_B(\nu_A-1)-\nu_A+2\right]\\
&\quad+\left[16-(16-\pi^2)\mu_B\right]\sqrt{1-\nu_A}\nu_A\Big\}^2\Bigg\}^{1/2}. \qquad (39)
\end{aligned}$$

Figure 1 is the density plots of $\overline{F}_{B\gamma,opt}$ in the μ_B-ν_γ space that clearly displays the domain in which the quantum protocol is useful (i.e., the optimal averaged fidelity of the JRSP of a 2-qubit state exceeds the classical limit equal to $2/5$ [51]).

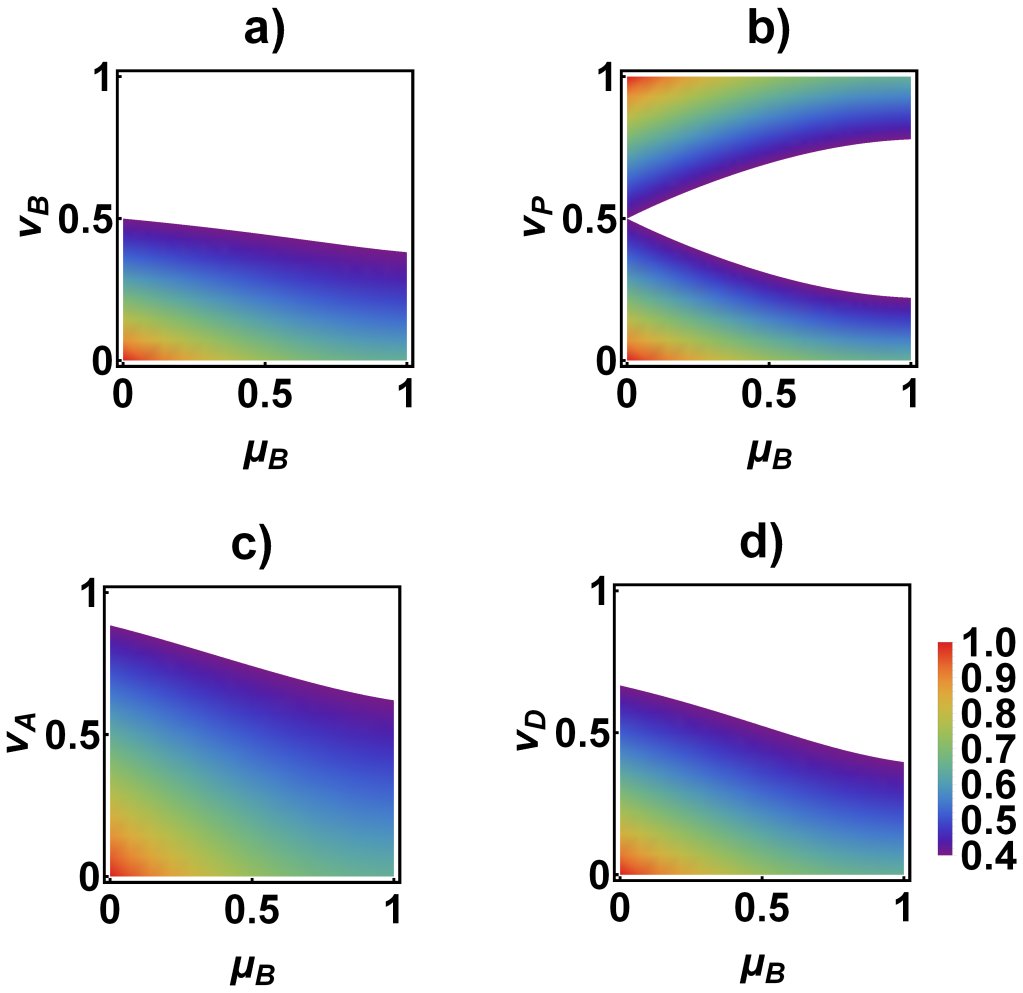

Fig. 1. Phase diagrams of the optimal averaged fidelities a) $\overline{F}_{BB,opt}$, b) $\overline{F}_{BP,opt}$, c) $\overline{F}_{BA,opt}$, and d) $\overline{F}_{BD,opt}$ in the $\mu_B - \nu_\gamma$ spaces. Colors illustrate the values of $\overline{F}_{B\gamma,opt}$ belonging to the quantum domain (i.e., $\overline{F}_{B\gamma,opt} > 2/5$), while white background shows the classical domain (i.e., $\overline{F}_{B\gamma,opt} < 2/5$).

Roughly speaking, from Figs. 1a, 1c and 1d, an increase in μ_B or/and ν_γ leads to a decrease in $\overline{F}_{B\gamma,opt}$. This means that with a given bit-flip noise acting on qubits 1 and 2, no matter the bit-flip, amplitude-damping or depolarizing noise is added to qubits 5 and 6, the quality of the protocol will become worse. For any value of μ_B there is always a chance to obtain the optimal averaged fidelities $\overline{F}_{B\gamma,opt}$ in quantum domain (i.e. the area in which $\overline{F}_{B\gamma,opt} > 2/5$), while there exists a limit

of the values of ν_γ, denoted as ν_γ^{lim}, from which for any $\nu_\gamma \geq \nu_\gamma^{lim}$ the protocol is no longer useful (i.e., $\overline{F}_{B\gamma,opt} \leq 2/5$). It can be understood that a greater value of ν_γ^{lim} is equivalent to a weaker influence of γ-type noise on the protocol. Comparing three Figs. 1a, 1c and 1d in more depth, one can see that $\nu_A^{lim} > \nu_D^{lim} > \nu_B^{lim}$ and the area of the quantum domain for $\gamma = A$ is the biggest and that for $\gamma = B$ is the smallest. Different from the quantum domains of $\overline{F}_{BB,opt}$, $\overline{F}_{BA,opt}$ and $\overline{F}_{BD,opt}$, the optimal averaged fidelity $\overline{F}_{BP,opt}$ in Fig. 1b is symmetric with respect to the segment $\nu_P = 1/2$, which results in the fact that a nonclassical fidelity can be obtained even in the region of strong noise strengths. Such symmetry was found in Refs. [41, 47], however, in this context it can be clearly shown from Eq. (37) in which $\overline{F}_{BP,opt}(\mu_B, 1/2 - \Delta\nu_P) = \overline{F}_{BP,opt}(\mu_B, 1/2 + \Delta\nu_P)$ with $0 \leq \Delta\nu_P \leq 1/2$ and its physical origin can be explained as follows. Without loss of generality we consider the scenario in which qubits 1 and 2 are not subjected to any noises, but qubits 5 and 6 at the same time are affected by the phase-flip noise with noisy strength p_P. It is necessary to recall the action of the phase-flip noise on a qubit: it flips the phase of the qubit being in the excited state with probability of p_P and lets the ground state unchanged with the probability of $1 - p_P$ [49]. For convenience, let us denote $\rho_{135\,(246)}^{(+)} = |GHZ_+\rangle_{135\,(246)}\langle GHZ_+|$ and $\rho_{135\,(246)}^{(-)} = |GHZ_-\rangle_{135\,(246)}\langle GHZ_-|$. In the case of $p_P < 1/2$, according to Eq. (32), the value of θ in Eq. (17) is chosen as $\pi/4$. Then after being subjected to the phase-flip noise the initial quantum channel $\left|Q(\frac{\pi}{4})\right\rangle_{135246}\left\langle Q(\frac{\pi}{4})\right|$ turns out to be a mixed state $(1-p_P)^2\rho_{135}^{(+)} \otimes \rho_{246}^{(+)} + p_P(1-p_P)\rho_{135}^{(+)} \otimes \rho_{246}^{(-)} + p_P(1-p_P)\rho_{135}^{(-)} \otimes \rho_{246}^{(+)} + p_P^2\rho_{135}^{(-)} \otimes \rho_{246}^{(-)}$. This implies that if p_P is approaching to 0, the noise-induced quantum channel is becoming closer and closer to $\rho_{135}^{(+)} \otimes \rho_{246}^{(+)}$, which is the quantum channel in the noiseless case (Eq. (10)). Therefore, it can be seen that with $\theta = \xi = \pi/4$, the smaller value of p_P the better the performance of the JRSP protocol. Next, in case p_P is larger than $1/2$, according to Eq. (32), θ in Eq. (17) is optimally chosen as $-\pi/4$. Similar to the preceding case, the effect of the phase-flip noise is to transform the initial pure quantum channel to a mixed state $p_P(1-p_P)\rho_{135}^{(+)} \otimes \rho_{246}^{(+)} + (1-p_P)^2\rho_{135}^{(+)} \otimes \rho_{246}^{(-)} + p_P^2\rho_{135}^{(-)} \otimes \rho_{246}^{(+)} + p_P(1-p_P)\rho_{135}^{(-)} \otimes \rho_{246}^{(-)}$. Now, it is clear that a larger value of p_P leads the initial quantum channel closer to the state $\rho_{135}^{(-)} \otimes \rho_{246}^{(+)}$. However, one can check that in the noiseless case, with the quantum channel chosen as $|GHZ_-\rangle_{135} \otimes |GHZ_+\rangle_{246}$, which coincides with $\rho_{135}^{(-)} \otimes \rho_{246}^{(+)}$, the matrix in Eq. (12) and the operators in Eqs. (13) and (15) being unchanged and the matrix of Eq. (14) replaced by $\widetilde{V}$ with $\xi = -\pi/4$ in Eq. (18), the JRSP protocol is perfect. As a result, it can be said that with both θ and ξ chosen as $-\pi/4$, the larger p_P is the closer the noisy JRSP protocol is to the perfect one. Based on the above explanation, it is not difficult to check that in order to obtain a quantum averaged fidelity larger than $2/5$ even in the domain of bit-flip noise strength Bob should first apply the Pauli operator X to the qubits before sending them via bit-flip environments. The results of this scheme illustrated in Fig. 2 show that all the averaged fidelities amount to 1 at $(\mu_B, \nu_B) = (1,1)$ or $(\mu_B, \nu_\gamma) = (1,0)$ for $\gamma \neq B$. Hence, different from the results of Refs. [41, 47] in case of the bit-flip noise, our scheme here can raise the fidelity when the noisy strength is considerable. In addition to suitable selection of μ_B and ν_A, the choice of $\theta^{(BA)}$ to be $\theta_{opt}^{(BA)} \neq \pi/4$ as in Eq. (33) at which the state of qubits $2,4$ and 6 becomes maximally entangled, implying a better quality of the JRSP for a lesser amount of shared entanglement. This somewhat surprising result was also seen in quantum teleportation [41] and JRSP of a 1-qubit state [47]. That is to say, application of the

Pauli operator before transmitting qubits and choice of appropriate value of $\theta^{(B\gamma)}$ can be regarded as a way to cope with noise caused by the environment.

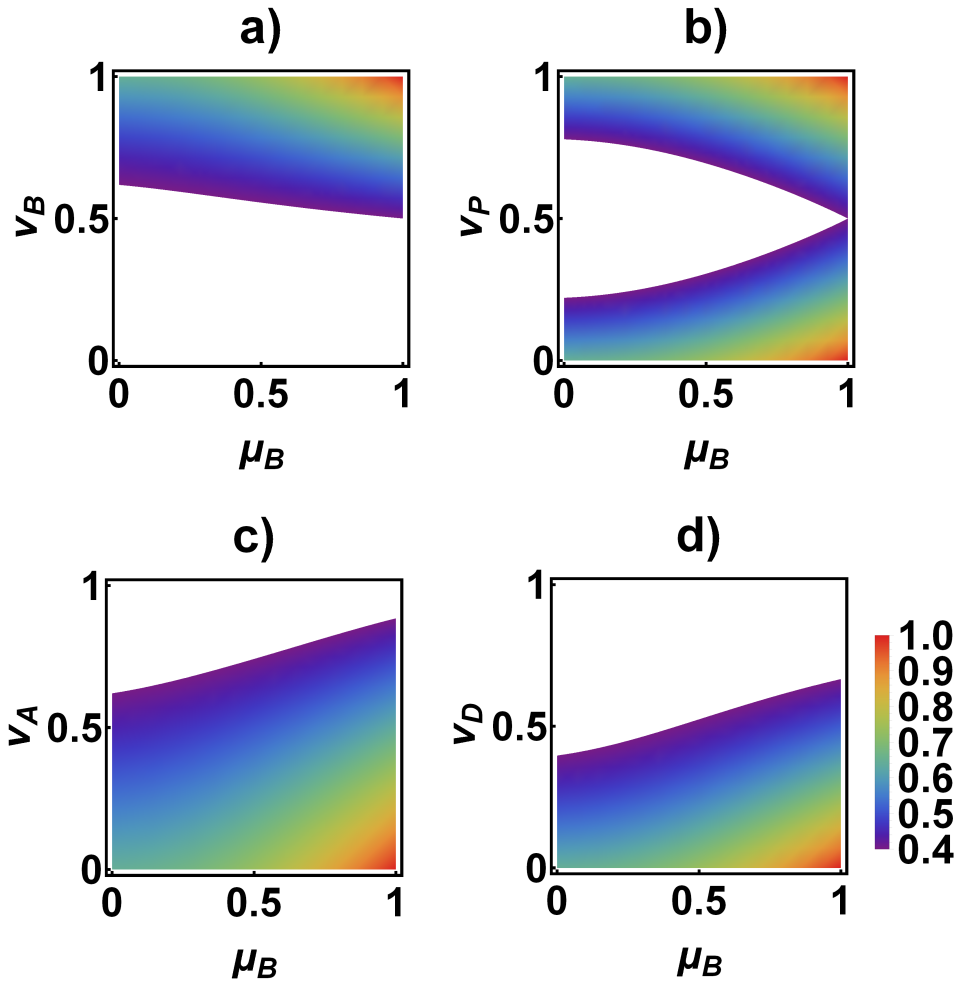

Fig. 2. Phase diagrams of the optimal averaged fidelities a) $\overline{F}_{BB,opt}$, b) $\overline{F}_{BP,opt}$, c) $\overline{F}_{BA,opt}$, and d) $\overline{F}_{BD,opt}$ in the $\mu_B - \nu_\gamma$ spaces in case all qubits subjected to bit-flip noise are applied to the Pauli operator X before being sent through noisy environments. Colors illustrate the values of $\overline{F}_{B\gamma,opt}$ belonging to the quantum domain (i.e., $\overline{F}_{B\gamma,opt} > 2/5$), while white background shows the classical domain (i.e., $\overline{F}_{B\gamma,opt} < 2/5$).

Next, consider $\alpha = P$ and $\gamma \in \{B,P,A,D\}$. The optimal averaged fidelities $\overline{F}_{P\gamma,opt}$ are achieved with the following values of $\theta_{opt}^{(P\gamma)}$ and $\xi_{opt}^{(P\gamma)}$:

$$\theta_{opt}^{(PB)} = \xi_{opt}^{(PB)} = \theta_{opt}^{(PD)} = \xi_{opt}^{(PD)} = \xi_{opt}^{(PA)} = \begin{cases} \pi/4 & \text{for } \mu_P < 1/2, \\ -\pi/4 & \text{for } \mu_P > 1/2, \end{cases} \tag{40}$$

$$\theta_{opt}^{(PP)} = \xi_{opt}^{(PP)} = \begin{cases} \pi/4 & \text{for } (1-2\mu_P)(1-2\nu_P) > 0, \\ -\pi/4 & \text{for } (1-2\mu_P)(1-2\nu_P) < 0, \end{cases} \tag{41}$$

$$\theta_{opt}^{(PA)} = \frac{1}{2}\arctan\frac{2\left(1-2\mu_P\right)\sqrt{1-\nu_A}}{\nu_A} \tag{42}$$

with $\sin 2\theta_{opt}^{(PA)} > 0$ and $\cos 2\theta_{opt}^{(PA)} > 0$ for $\mu_P < 1/2$ or $\sin 2\theta_{opt}^{(PA)} < 0$ and $\cos 2\theta_{opt}^{(PA)} > 0$ for $\mu_P > 1/2$. The explicit expressions of $\overline{F}_{P\gamma,opt}$ are collected in the Appendix.

From Fig. 3 one sees that the useful regions in Figs. 3a, 3c and 3d have similar patterns with the symmetry with respect to the segment $\mu_P = 1/2$. However, the quantum area for $\overline{F}_{PA,opt}$ is greater than those for either $\overline{F}_{PB,opt}$ or $\overline{F}_{PD,opt}$. Moreover, Fig. 3b shows that the quantum area is symmetric with respect not only to the segment $\mu_P = 1/2$ but also to the segment $\nu_P = 1/2$ and it spreads over the full parameter range. This, therefore, is an interesting result since no matter how strong noises are the protocol is always useful. The reason for those symmetries is similar to what explained in Fig. 1b and the quantum domain of $\overline{F}_{PB,opt}$ can be found in a bigger range of ν_B by employing the same scheme whose result is demonstrated in Fig. 2. It is noteworthy to stress that the value of $\theta_{opt}^{(PA)}$ in Eq. (42) does not need to be equal to $\pi/4$, again implying that a better quality of the JRSP is obtained by using an initial quantum channel with nonmaximal degree of entanglement.

Now, address the scenario in which $\alpha = A$ and $\gamma \in \{B,P,A,D\}$. The values of $\theta_{opt}^{(A\gamma)}$ and $\xi_{opt}^{(A\gamma)}$ can be derived as

$$\xi_{opt}^{(AB)} = \xi_{opt}^{(AA)} = \xi_{opt}^{(AD)} = \frac{\pi}{4}, \tag{43}$$

$$\theta_{opt}^{(AB)} = \frac{1}{2}\arctan\frac{\left(1-\nu_B\right)^2\left\{\sqrt{1-\mu_A}\left[\left(\pi^2-16\right)\mu_A+32\right]+32\left(1-\mu_A\right)\right\}}{\mu_A\left\{\left(16-\pi^2\right)\sqrt{1-\mu_A}\left(1-\nu_B\right)^2-8\left(2\nu_B-1\right)\left[2\left(\mu_A-1\right)\nu_B-\mu_A+2\right]\right\}} \tag{44}$$

with $\sin 2\theta_{opt}^{(AB)} > 0$ and $\cos 2\theta_{opt}^{(AB)} > 0$ for μ_A, ν_B satisfying the inequality

$$\left(16-\pi^2\right)\sqrt{1-\mu_A}\left(1-\nu_B\right)^2-8\left(2\nu_B-1\right)\left[2\left(\mu_A-1\right)\nu_B-\mu_A+2\right] > 0$$

or with $\sin 2\theta_{opt}^{(AB)} > 0$ and $\cos 2\theta_{opt}^{(AB)} < 0$ for μ_A, ν_B satisfying the inequality

$$\left(16-\pi^2\right)\sqrt{1-\mu_A}\left(1-\nu_B\right)^2-8\left(2\nu_B-1\right)\left[2\left(\mu_A-1\right)\nu_B-\mu_A+2\right] < 0, \tag{45}$$

$$\theta_{opt}^{(AA)} = \frac{1}{2}\arctan\frac{M_{AA}}{N_{AA}} \tag{46}$$

with $\sin 2\theta_{opt}^{(AA)} > 0$ and $\cos 2\theta_{opt}^{(AA)}$ for any μ_A, ν_A and

$$\begin{aligned} M_{AA} &= \frac{1}{160}\Big\{\sqrt{\left(\mu_A-1\right)\left(\nu_A-1\right)}\left[32-\left(\pi^2-16\right)\mu_A\left(\nu_A-1\right)-16\nu_A\right] \\ &\quad +32\left(\mu_A-1\right)\left(\nu_A-1\right)\Big\}, \end{aligned} \tag{47}$$

$$\begin{aligned} N_{AA} &= \frac{1}{160}\Big\{\sqrt{\left(\mu_A-1\right)\left(\nu_A-1\right)}\left[\left(\pi^2-16\right)\mu_A\left(\nu_A-1\right)+16\nu_A\right] \\ &\quad +8\left[\mu_A(1-2\nu_A)+\nu_A\right]\left[\mu_A\left(2\nu_A-1\right)+2-\nu_A\right]\Big\}, \end{aligned} \tag{48}$$

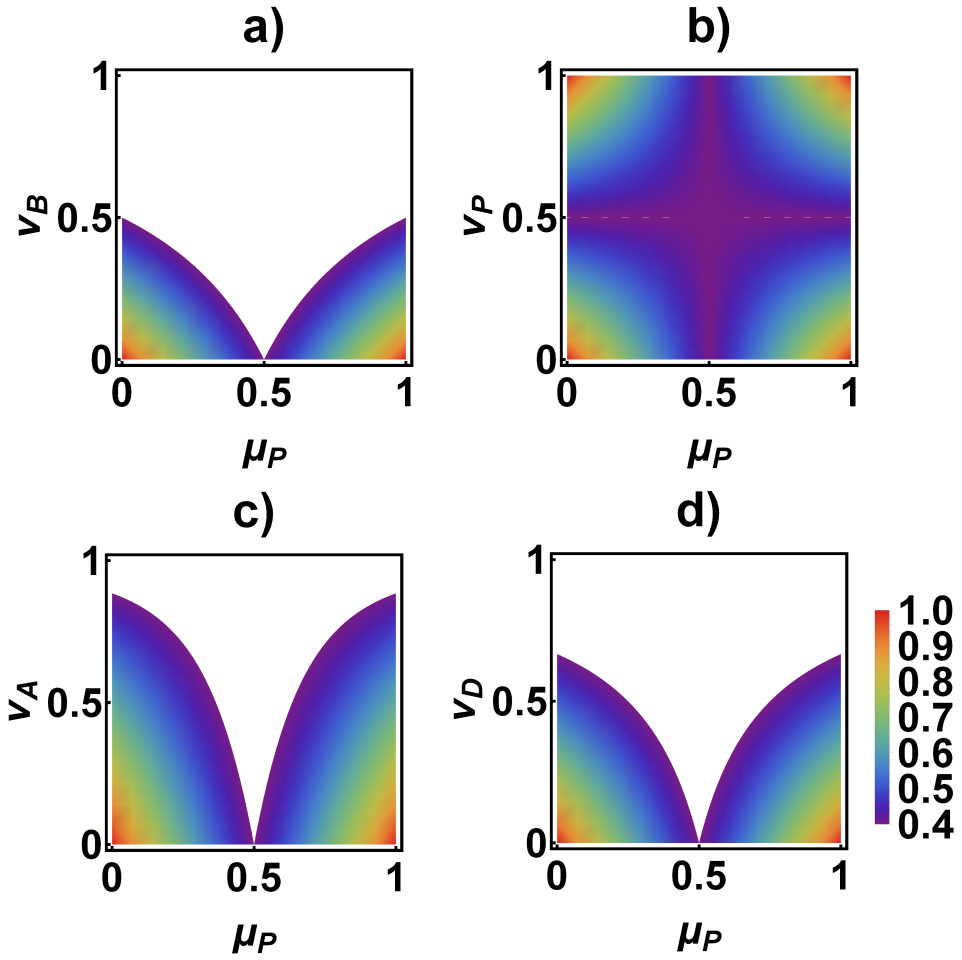

Fig. 3. Phase diagrams of the optimal averaged fidelities a) $\overline{F}_{PB,opt}$, b) $\overline{F}_{PP,opt}$, c) $\overline{F}_{PA,opt}$, and d) $\overline{F}_{PD,opt}$ in the $\mu_P - \nu_\gamma$ spaces. Colors illustrate the values of $\overline{F}_{P\gamma,opt}$ belonging to the quantum domain (i.e., $\overline{F}_{P\gamma,opt} > 2/5$), while white background shows the classical domain (i.e., $\overline{F}_{P\gamma,opt} < 2/5$).

$$\theta_{opt}^{(AD)} = \frac{1}{2}\arctan\frac{\sqrt{1-\mu_A}\left[(\pi^2-16)\mu_A+32\right](2-\nu_D)+64(\mu_A-1)(\nu_D-1)}{\mu_A\left\{\left[(16-\pi^2)\sqrt{1-\mu_A}+16\right](2-\nu_D)+16\mu_A(\nu_D-1)\right\}}$$

with $\sin 2\theta_{opt}^{(AD)} > 0$ and $\cos 2\theta_{opt}^{(AD)} > 0$ for any $0 < \mu_A \leq 1$ and $0 \leq \nu_D < 1$,

$$\xi_{opt}^{(AP)} = \begin{cases} \pi/4 & \text{for } \nu_P < 1/2, \\ -\pi/4 & \text{for } \nu_P > 1/2, \end{cases} \tag{49}$$

$$\theta_{opt}^{(AP)} = \frac{1}{2}\arctan\frac{(1-2\nu_P)\left\{32(\mu_A-1)(2\nu_P-1)+\sqrt{1-\mu_A}\left[(\pi^2-16)\mu_A+32\right]\right\}}{\mu_A\left[(\pi^2-16)\sqrt{1-\mu_A}(2\nu_P-1)-8\mu_A+16\right]}$$

with $\sin 2\theta_{opt}^{(AP)} > 0$ and $\cos 2\theta_{opt}^{(AP)} > 0$ for $\nu_P < 1/2$ or with $\sin 2\theta_{opt}^{(AP)} < 0$ and $\cos 2\theta_{opt}^{(AP)} > 0$ for $\nu_P > 1/2$. The explicit expressions of $\overline{F}_{A\gamma,opt}$ are given in the Appendix.

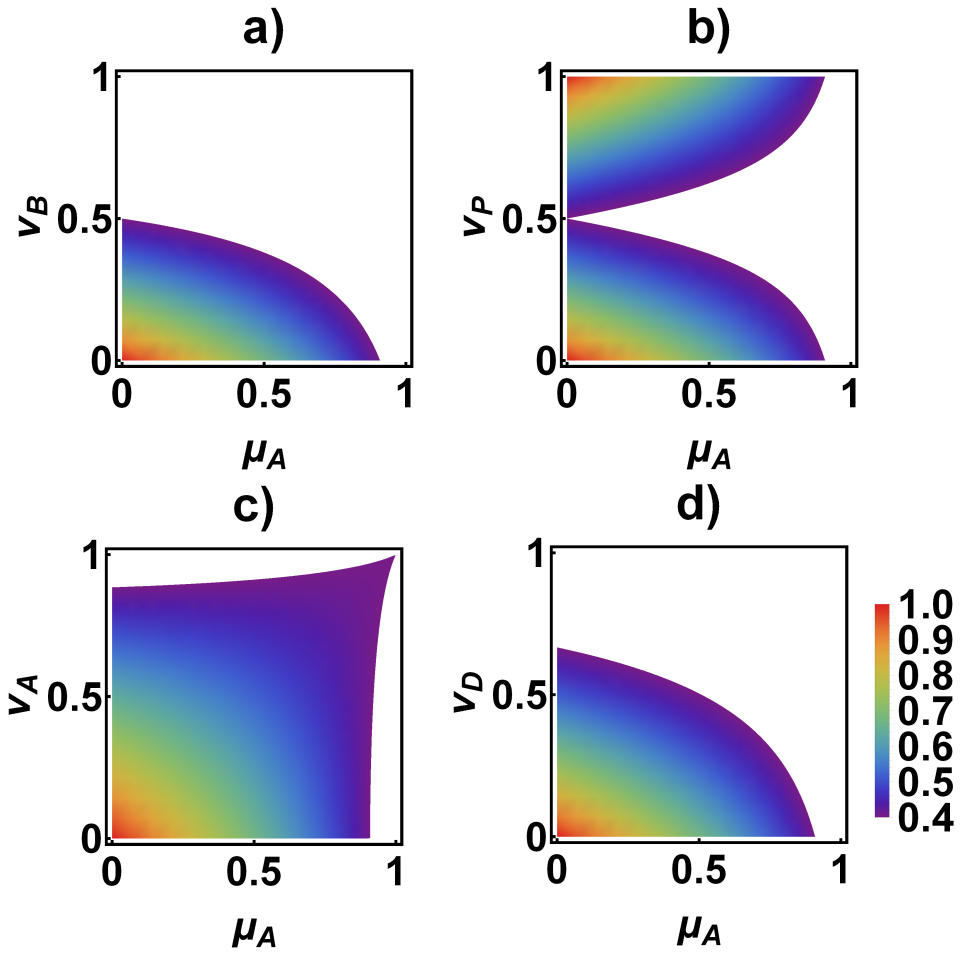

Fig. 4. Phase diagrams of the optimal averaged fidelities a) $\overline{F}_{AB,opt}$, b) $\overline{F}_{AP,opt}$, c) $\overline{F}_{AA,opt}$, and d) $\overline{F}_{AD,opt}$ in the $\mu_A - \nu_\gamma$ spaces. Colors illustrate the values of $\overline{F}_{A\gamma,opt}$ belonging to the quantum domain (i.e., $\overline{F}_{A\gamma,opt} > 2/5$), while white background shows the classical domain (i.e., $\overline{F}_{A\gamma,opt} < 2/5$).

As seen from Fig. 4, since the quantum domain spreads over almost all values of noise strengths, the value of $\overline{F}_{AA,opt}$ appears larger than $\overline{F}_{AB,opt}$, $\overline{F}_{AP,opt}$ and $\overline{F}_{AD,opt}$. Furthermore, while $\overline{F}_{AB,opt}$ and $\overline{F}_{AD,opt}$ decrease with any rise in noise strengths, there is a region in which $\overline{F}_{AA,opt}$ is found to be greater even with stronger noise strengths. The above result is similar to the ones obtained for quantum teleportation in Refs. [37, 39].

Finally, the scenario with $\alpha = D$ and $\gamma \in \{B,P,A,D\}$ has the results as follows

$$\theta_{opt}^{(DB)} = \xi_{opt}^{(DB)} = \theta_{opt}^{(DD)} = \xi_{opt}^{(DD)} = \xi_{opt}^{(DA)} = \frac{\pi}{4}, \tag{50}$$

$$\theta_{opt}^{(DP)} = \xi_{opt}^{(DP)} = \begin{cases} \pi/4 & \text{for } \nu_P < 1/2, \\ -\pi/4 & \text{for } \nu_P > 1/2, \end{cases} \tag{51}$$

$$\theta_{opt}^{(DA)} = \frac{1}{2}\arctan\frac{\left[(\pi^2-16)\mu_D+32\right]\sqrt{1-\nu_A}\,(2-\nu_A)+64\,(\mu_D-1)\,(\nu_A-1)}{\nu_A\left\{\left[(\pi^2-16)\mu_D+32\right]\sqrt{1-\nu_A}+16\left[\mu_D\,(\nu_A-1)-\nu_A+2\right]\right\}} \tag{52}$$

with $\sin 2\theta_{opt}^{(DA)} > 0$ and $\cos 2\theta_{opt}^{(DA)} > 0$ for any $0 \le \mu_D < 1$ and $0 < \nu_A \le 1$. The explicit expressions of $\overline{F}_{D\gamma,opt}$ are provided in the Appendix.

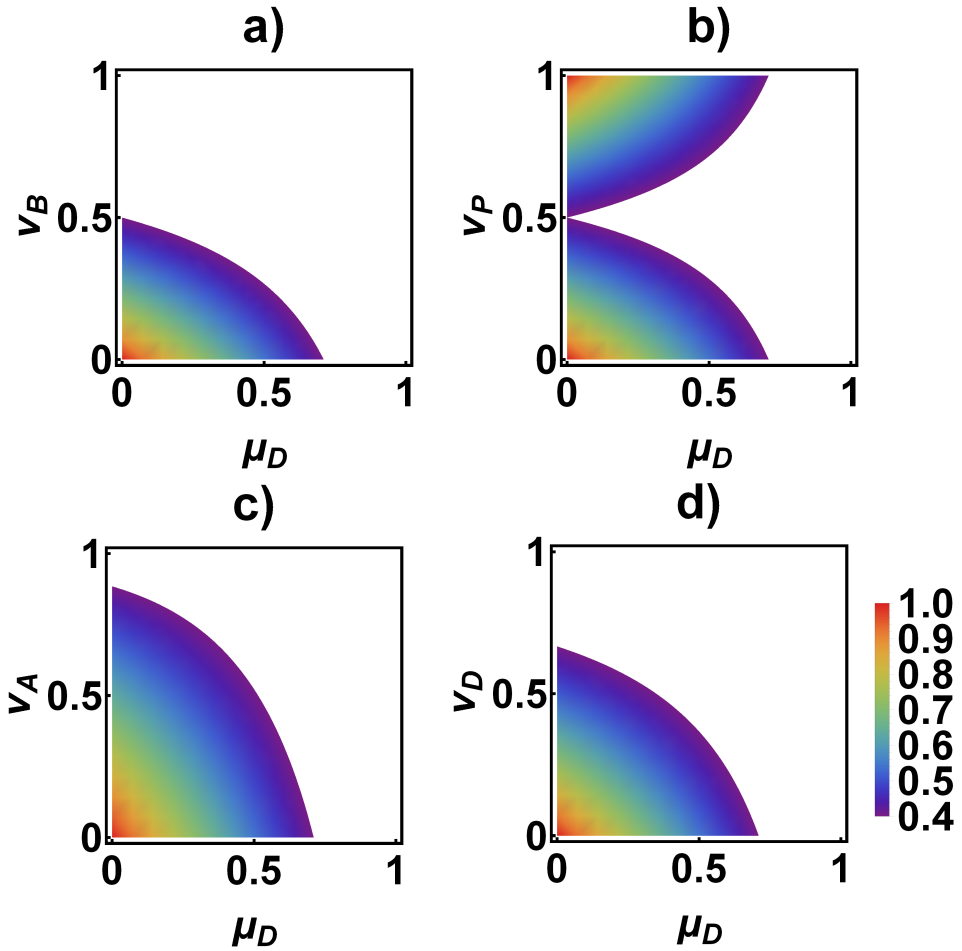

Fig. 5. Phase diagram of the optimal averaged fidelities a) $\overline{F}_{DB,opt}$, b) $\overline{F}_{DP,opt}$, c) $\overline{F}_{DA,opt}$, and d) $\overline{F}_{DD,opt}$ in the $\mu_D - \nu_\gamma$ spaces. Colors illustrate the values of $\overline{F}_{D\gamma,opt}$ belonging to the quantum domain (i.e., $\overline{F}_{D\gamma,opt} > 2/5$), while white background shows the classical domain (i.e., $\overline{F}_{D\gamma,opt} < 2/5$).

As shown in Fig. 5, the quantum area of $\overline{F}_{DA,opt}$ keeps superior to those of $\overline{F}_{DB,opt}$ and $\overline{F}_{DD,opt}$ and there is a symmetry at the change of $\overline{F}_{DP,opt}$.

IV. CONCLUSION

With the assumption of 2 qubits of either the first or the second preparer being affected by noises during the process of distribution of the initial quantum channel, we have tried to find a way to enhance the averaged fidelity of the JRSP of an arbitrary 2-qubit state. The noises concerned include the bit-flip, phase-flip, amplitude-damping and depolarizing. To describe the effect of such noises, superoperators in form of sums of Kraus operators are exploited. By introducing in the initial quantum channel and the basis measurement of the second preparer two parameters which are controllable versus the strength of given noises, the averaged fidelities are optimized in different noisy scenarios. Then the results of the optimization are represented in phase-space diagrams to clarify visually the noise domain in which the optimal averaged fidelity is greater than the classical limit. Through analyzing the diagrams we have encountered the symmetrical character of the optimal averaged fidelity subjected to the phase-flip noise which is basically explained. Besides, the fidelity under the influence of the bit-flip noise is also optimized in a different manner: Bob, who produces the quantum channel, applies the Pauli operator X on qubits which are sent through bit-flip environments in case when he knows that the noise strength is strong. Essentially, depending on the range of noisy parameter, suitable values of the introduced control parameters θ and ξ can be chosen in case of the phase-flip noise or applying the Pauli operator X in case of the bit-flip noise so that to transform the initial state of qubits 1, 3 and 5 (2, 4 and 6) from one of the GHZ states into other GHZ states or to change Bob's measurement basis. Therefore, the optimization of the bit-flip noise as well as that of the phase-flip noise does not change the entanglement degree of the quantum channel. In contrast to this, the optimization for the JRSP affected by the amplitude-damping noise showed that the value of $\theta_{opt}^{(A\gamma)}$ or $\theta_{opt}^{(\alpha A)}$ is varied with the change of noise parameters and possibly being different from $\pi/4$, which in principle makes the entanglement of the quantum channel changed. Remarkably, when qubits 1 and 2 experience the amplitude-damping noise, adding another noise on qubits 5 and 6 can broaden the area of quantum domain even in considerable noise parameter ranges only when that noise is again amplitude-damping. Such optimization should be interpreted as the optimization which is accomplished through dissipative interactions with noisy environments. The obtained results might shed some light on ways of improving the realistic manipulation of JRSP.

ACKNOWLEDGMENTS

This work is supported by the Vietnam Foundation for Science and Technology Development (NAFOSTED) under a project no. 103.01-2017.08.

REFERENCES

[1] Y. Xia, J. Song and H. S. Song, *J. Phys. B: At. Mol. Opt. Phys.* **40** (2007) 3719.
[2] N. B. An and J. Kim, *J. Phys. B: At. Mol. Opt. Phys.* **41** (2008) 095501.
[3] N. B. An and J. Kim, *Int. J. Quant. Inf.* **6** (2008) 1051.
[4] A. K. Pati, *Phys. Rev. A* **63** (2000) 014302.
[5] N. B. An, *J. Phys. B: At. Mol. Opt. Phys.* **42** (2009) 125501.
[6] K. Hou, J. Wang, Y. L. Lu and S. H. Shi, *Int. J. Theor. Phys.* **48** (2009) 2005.

[7] M. X. Lou, X. B. Chen, S. Y. Ma, X. X. Niu and Y. X. Yang, *Opt. Commun.* **283** (2010) 4796.
[8] Q. Q. Chen, Y. Xia, J. Song and N. B. An, *Phys. Lett. A* **374** (2010) 4483.
[9] N. B. An, *Opt. Commun.* **283** (2010) 4113.
[10] N. B. An, C. T. Bich and N. V. Don, *Phys. Lett. A* **375** (2011) 3570.
[11] N. B. An, C. T. Bich and N. V. Don, *J. Phys. B: At. Mol. Opt. Phys.* **44** (2011) 135506.
[12] Q. Q. Chen, Y. Xia and N. B. An, *Opt. Commun.* **284** (2011) 2617.
[13] Z. Y. Wang, *Int. J. Quant. Inf.* **9** (2011) 809.
[14] K. Hou, Y. B. Li, G. H. Liu and S. Q. Sheng, *J. Phys. A: Math. Theor.* **44** (2011) 255304.
[15] X. Q. Xiao, J. M. Liu and G. Zeng, *J. Phys. B: At. Mol. Opt. Phys.* **44** (2011) 075501.
[16] C. T. Bich, N. V. Don and N. B. An, *Int. J. Theor. Phys.* **51** (2012) 2272.
[17] Y. Xia, Q. Q. Chen and N. B. An, *J. Phys. A: Math. Theor.* **45** (2012) 335306.
[18] M. X. Luo, J. Y. Peng and Z. W. Mo, *Int. J. Theor. Phys.* **52** (2013) 644.
[19] Y. B. Zhan and P. C. Ma, *Quant. Inf. Process.* **12** (2013) 997.
[20] Y. B. Zhan, H. Fu, X. W. Li and P. C. Ma, *Int. J. Theor. Phys.* **52** (2013) 2615.
[21] L. R. Long, P. Zhou, Z. Li and C. L. Yin, *Int. J. Theor. Phys.* **51** (2012) 2438.
[22] D. Wang and L. Ye, *Int. J. Theor. Phys.* **51** (2012) 3376.
[23] Y. M. Liao, P. Zhou, X. C. Qin and Y. H. He, *Quant. Inf. Process.* **13** (2014) 615.
[24] M. X. Luo, X. B. Chen, Y. X. Yang and X. X. Niu, *Quant. Inf. Process.* **11** (2012) 751.
[25] R. F. Yu, Y. J. Lin and P. Zhou, *Quant. Inf. Process.* **15** (2016) 4785.
[26] T. Yu and J. H. Eberly, *Phys. Rev. Lett.* **93** (2004) 140404; *Phys. Rev. Lett.* **97** (2006) 140403.
[27] N. B. An and J. Kim, *Phys. Rev. A* **79** (2009) 022303.
[28] C. H. Bennett, G. Brassard, S. Popescu, B. Schumacher, J. A. Smolin and W. K. Wooters, *Phys. Rev. Lett.* **76** (1996) 722.
[29] J. W. Pan, C. Simon, C. Brukner and A. Zeilinger, *Nature* **410** (2001) 1067.
[30] J. L. Romero, L. Roa, J. C. Retamal and C. Saavedra, *Phys. Rev. A* **65** (2002) 052319.
[31] Q. Sun, M. Al-Amri and M. S. Zubairy, *Phys. Rev. A* **80** (2009) 033838.
[32] J. C. Lee, Y. C. Jeong, Y. S. Kim and Y. H. Kim, *Opt. Express* **19** (2011) 16309.
[33] M. Hamada, *Phys. Rev. A* **68** (2003) 012301.
[34] T. Pramanik and A. S. Majumdar, *Phys. Lett. A* **377** (2013) 3209.
[35] L. Qiu, G. Tang, X. Yang and A. Wang, *Ann. Phys.* **350** (2014) 137.
[36] B. G. Taketani, F. de Melo and R. L. de Matos Filho, *Phys. Rev. A* **85** (2012) 020301.
[37] L. T. Knoll, Ch. T. Schmiegelow and M. A. Larotonda, *Phys. Rev. A* **90** (2014) 042332.
[38] P. Badziag, M. Horodecki, P. Horodecki and R. Horodecki, *Phys. Rev. A* **62** (2000) 012311.
[39] S. Bandyopadhyay, *Phys. Rev. A* **65** (2002) 022302.
[40] Y. Yeo, *Phys. Rev. A* **78** (2008) 022334.
[41] R. Fortes and G. Rigolin, *Phys. Rev. A* **92** (2015) 012338.
[42] H. Q. Liang, J. M. Liu, S. S. Feng, J. G. Chen and X. Y. Xu, *Quant. Inf. Process.* **14** (2015) 3857.
[43] Z. F. Chen, J. M. Liu and L. Ma, *Chin. Phys. B* **23** (2014) 020312.
[44] X. W. Guan, X. B. Chen, L. C. Wang and Y. X. Yang, *Int. J. Theor. Phys.* **53** (2014) 223.6
[45] M. M. Wang and Z. G. Qu, *Quant. Inf. Process.* **15** (2016) 4805.
[46] H. Zhao and L. Huang, *Int. J. Theor. Phys.* **56** (2017) 720.
[47] N. V. Hop, C. T. Bich and N. B. An, *Adv. Nat. Sci.: Nanosci. Nanotech.* **8** (2017) 015012.
[48] K. Kraus, *States, Effects and Operators: Fundamental Notions of Quantum Theory*, Springer-Verlag, Berlin, 1983.
[49] M. A. Nielsen and I. L. Chuang, *Quantum Computation and Quantum Information*, Cambridge University Press, Cambridge, 2000.
[50] K. Zyczkowski and H. J. Sommers, *J. Phys. A: Math. Gen.* **34** (2001) 7111.
[51] D. Bruß and C. Macchiavello, *Phys. Lett. A* **253** (1999) 249.

APPENDIX

The explicit expressions of $\overline{F}_{\beta\gamma,opt}$, with $\beta \in \{P,A,D\}$ and $\gamma \in \{P,B,A,D\}$, were derived and are shown in this appendix.

$$\overline{F}_{PB,opt} = \frac{2}{5}+\frac{1}{5}(\nu_B-2)\nu_B+\frac{1}{5}(2\mu_P-1)^2(\nu_B-1)^2+\frac{2}{5}(\nu_B-1)^2|1-2\mu_P|, \tag{53}$$

$$\overline{F}_{PP,opt} = \frac{2}{5}+\frac{1}{5}(2\mu_P-1)^2(2\nu_P-1)^2+\frac{2}{5}\big|(2\mu_P-1)(2\nu_P-1)\big|, \tag{54}$$

$$\begin{aligned}\overline{F}_{PA,opt} &= \frac{2}{5}+\frac{1}{20}(\nu_A-4)\nu_A+\frac{1}{10}\sqrt{1-\nu_A}(2-\nu_A)|1-2\mu_P| \\ &\quad +\frac{1}{20}\Bigg\{\Big\{2(1-2\mu_P)\big[2(1-\nu_A)|1-2\mu_P|+\sqrt{1-\nu_A}(2-\nu_A)\big]\Big\}^2 \\ &\quad +\Big\{\nu_A\big[2\sqrt{1-\nu_A}|1-2\mu_P|+2-\nu_A\big]\Big\}^2\Bigg\}^{1/2},\end{aligned} \tag{55}$$

$$\overline{F}_{PD,opt} = \frac{2}{5}+\frac{1}{20}(\nu_D-4)\nu_D+\frac{1}{5}(2\mu_P-1)^2(\nu_D-1)^2+\frac{1}{5}(\nu_D-2)(\nu_D-1)|1-2\mu_P|, \tag{56}$$

$$\begin{aligned}\overline{F}_{AB,opt} &= \frac{2}{5}+\frac{1}{160}\Big\{\sqrt{1-\mu_A}\big[(\pi^2-16)\mu_A+32\big](\nu_B-1)^2 \\ &\quad +8\big[2(\mu_A-1)\nu_B-\mu_A\big]\big[2(\mu_A-1)\nu_B-\mu_A+4\big]\Big\} \\ &\quad +\frac{1}{160}\Bigg\{\mu_A^2\Big\{\big(16-\pi^2\big)\sqrt{1-\mu_A}(\nu_B-1)^2+8(1-2\nu_B)\big[2(\mu_A-1)\nu_B-\mu_A+2\big]\Big\}^2 \\ &\quad +(\nu_B-1)^4\big[32-32\mu_A+\sqrt{1-\mu_A}(\pi^2\mu_A-16\mu_A+32)\big]^2\Bigg\}^{1/2},\end{aligned} \tag{57}$$

$$\begin{aligned}\overline{F}_{AP,opt} &= \frac{2}{5}+\frac{1}{20}(\mu_A-4)\mu_A+\frac{1}{160}\sqrt{1-\mu_A}\big[(\pi^2-16)\mu_A+32\big]|1-2\nu_P| \\ &\quad +\frac{1}{160}\Bigg\{(1-2\nu_P)^2\Big\{\sqrt{1-\mu_A}\big[(\pi^2-16)\mu_A+32\big]+32(1-\mu_A)|1-2\nu_P|\Big\}^2 \\ &\quad +\mu_A^2\big[(16-\pi^2)\sqrt{1-\mu_A}|1-2\nu_P|+8(2-\mu_A)\big]^2\Bigg\},\end{aligned} \tag{58}$$

$$\begin{aligned}\overline{F}_{AA,opt} &= \frac{2}{5}+\frac{1}{160}\Big\{\sqrt{(\mu_A-1)(\nu_A-1)}\big[32-(\pi^2-16)\mu_A(\nu_A-1)-16\nu_A\big] \\ &\quad +8\big[\mu_A(2\nu_A-1)-\nu_A\big]\big[\mu_A(2\nu_A-1)-\nu_A+4\big]\Big\}+\big(M_{AA}^2+N_{AA}^2\big)^{1/2}\end{aligned} \tag{59}$$

with M_{AA} and N_{AA} defined as in Eqs. (47) and (48),

$$\begin{aligned}
\overline{F}_{AD,opt} &= \frac{2}{5}+\frac{1}{320}\Big\{16\big[(\mu_A(\nu_D-1)-\nu_D\big]\big[\mu_A(\nu_D-1)-\nu_D+4\big] \\
&\quad +\sqrt{1-\mu_A}\big[(\pi^2-16)\mu_A+32\big](\nu_D-2)(\nu_D-1)\Big\} \\
&\quad +\frac{1}{320}\Bigg\{(1-\nu_D)^2\Big\{\sqrt{1-\mu_A}\big[(\pi^2-16)\mu_A+32\big](2-\nu_D)+64(\mu_A-1)(\nu_D-1)\Big\}^2 \\
&\quad +\mu_A^2(1-\nu_D)^2\Big\{\big[(16-\pi^2)\sqrt{1-\mu_A}+16\big](2-\nu_D)+16\mu_A(\nu_D-1)\Big\}^2\Bigg\}^{1/2}, \quad (60)\\
\overline{F}_{DB,opt} &= \frac{2}{5}+\frac{1}{80}\Bigg\{4\Big\{\mu_D^2\big[4\nu_B(3\nu_B-5)+9\big]-4\mu_D(\nu_B-1)(7\nu_B-6) \\
&\quad +4\big[4(\nu_B-2)\nu_B+3\big]\Big\}+\pi^2(1-\mu_D)\mu_D(\nu_B-1)^2\Bigg\}, \quad (61)\\
\overline{F}_{DP,opt} &= \frac{2}{5}+\frac{1}{80}\Big\{(1-\mu_D)\big[(\pi^2-16)\mu_D+32\big]|1-2\nu_P|+16(\mu_D-1)^2(1-2\nu_P)^2 \\
&\quad +4\mu_D^2-16\mu_D\Big\}, \quad (62)\\
\overline{F}_{DA,opt} &= \frac{2}{5}+\frac{1}{320}\Big\{(1-\mu_D)\big[(\pi^2-16)\mu_D+32\big]\sqrt{1-\nu_A}(2-\nu_A) \\
&\quad +16\big[\mu_D(\nu_A-1)-\nu_A\big]\big[\mu_D(\nu_A-1)-\nu_A+4\big]\Big\} \\
&\quad +\frac{1}{320}\Bigg\{(1-\mu_D)^2\Big\{\big[(\pi^2-16)\mu_D+32\big]\sqrt{1-\nu_A}(2-\nu_A)+64(1-\mu_D)(1-\nu_A)\Big\}^2 \\
&\quad +(1-\mu_D)^2\nu_A^2\Big\{\big[(\pi^2-16)\mu_D+32\big]\sqrt{1-\nu_A}+16\big[\mu_D(\nu_A-1)-\nu_A+2\big]\Big\}^2\Bigg\}^{1/2}, \\
&\quad (63)\\
\overline{F}_{DD,opt} &= \frac{2}{5}+\frac{1}{160}\Big\{8\big[\mu_D^2(\nu_D-1)(7\nu_D-9)-8\mu_D(\nu_D-1)(2\nu_D-3) \\
&\quad +3(\nu_D-2)(3\nu_D-2)\big]+\pi^2(1-\mu_D)\mu_D(2-\nu_D)(1-\nu_D)\Big\}. \quad (64)
\end{aligned}$$